Photoinduced Reactions in the Ion−Molecule Complexes Mg^+-XCH_3 (X = F, Cl)

Xin Yang, Yihua Hu, and Shihe Yang*

Department of Chemistry, The Hong Kong University of Science and Technology, Clear Water Bay, Kowloon, Hong Kong

Received: March 10, 2000; In Final Form: June 20, 2000

The cation−molecule complexes $Mg^+-(XCH_3)_n$ (X = F, Cl) were produced in a laser-ablation pickup source. Photoinduced reactions in Mg^+-FCH_3 and Mg^+-ClCH_3 were observed, with the dominant or the only products being CH_3^+ and MgX. We have measured the relative photodissociation product yields as a function of the excitation wavelength for several complexes in a broad spectral region. Experiments on the complexes with different halide substitutions show different photoreaction patterns. In particular, photodissociation of the cationic complex Mg^+-FCH_3 produced exclusively MgF and CH_3^+, whereas in Mg^+-ClCH_3, nonreactive quenching was also observed besides the reactive channel mentioned above. The photodissociation action spectra are discussed with the help of quantum ab initio calculations of both the ground state and the relevant excited-state potential energy surfaces.

I. Introduction

The reactions between molecules in restricted geometries have received considerable interest during the past decade.[1−4] The primary goal is to control such attributes as the impact parameter, angle of approach, and relative kinetic energy and internal energy of the reactants involved, which dictate the final outcome of a given reaction. The transition state configuration, which is intermediate between reactants and products, can be accessed through optical excitation into excited states with nuclear coordinates pre-defined by the ground-state structure. This type of transition state spectroscopy has been extensively applied to negative ions,[5] neutral complexes,[6−9] and surface-aligned species [10] in domains of both frequency and real time.[11]

Photodissociation spectroscopy of metal cation−molecule complexes is potentially a useful means to explore the potential energy surfaces in the transition state region of excited-state reactions.[12] There are several advantages in this pursuit. First of all, the charged species (both reactants and products) can be detected with nearly unit efficiency and mass-analyzed rapidly by time-of-flight mass spectrometry.[13,14] Next, the ion−molecule complexes are often easy to generate in comparison with their neutral counterparts. This is due to the relatively stronger electrostatic binding forces. More importantly, owing to this moderate binding energy between the cation and the molecule in a cation−molecule complex, excited-state reactions can be started with a clear-cut geometry in contrast to the floppy nature of neutral van der Waals complexes. The fixed geometry of the cation−molecule complex ensures a well-defined starting point (e.g., relative electronic orbital alignment, collision energy, and angular momentum) for trajectories to evolve after optical excitation. The product branching ratios resulting from these photoinduced reactions, when measured as a function of the excitation photon energy, may provide important information on the complex structure and dynamics pertaining to the excited-state potential energy surfaces, i.e., nonadiabatic couplings, tunneling interactions, stereo-dynamic effects, etc. Finally, the structures of the cation−molecule complexes are often amenable to present-day quantum ab initio calculations and spectroscopic measurements.

Singly charged alkaline earth metal cations are iso-electronic to the alkali metal atoms, which played an important role in early days (the alkali age) of reaction dynamics.[15] They have substantial oscillator strengths in the visible and ultraviolet spectral regions, which can be easily accessed by pulsed laser sources.[16] The existence of one valence electron in an alkaline metal cation gives rise to the possibility of nonadiabatic interactions. Depending on the bonding properties of the molecule in a metal cation−molecule complex, the outcome of the nonadiabatic interactions can be chemical reactions or nonreactive quenching processes. The study of mass-selected cation−molecule complexes allows a direct measurement of the quantum yields for the competing reactive and nonreactive quenching processes in a given "half-reaction".[12]

Previous studies on photodissociation of metal cation−molecule complexes were mainly directed to understand solvation phenomena.[17−20] More recently, photoinduced reactions on some of these systems, which involve the activation of C═O, H−H, C−H, and O−H bonds, were observed and investigated.[21−24] Kleiber et al. proposed a bond-stretch mechanism for photoinduced reactions in complexes of alkaline earth metal ion and H_2 or hydrocarbons.[22] Farrar and co-workers studied the photodissociation of $Sr^+(CH_3OH)/Sr^+(CH_3OD)$ and $SrOH^+/SrOD^+$. For the $Sr^+(H_2O)_n$ and $Sr^+(D_2O)_n$ systems, the authors found that photodissociation of all the clusters result in both ligand loss and H/D elimination.[21] Careful examination of the product branching revealed that rapid internal conversion followed by an intracluster reaction preferentially occurred on the ground-state surface, while evaporation occurred primarily in the excited state. Fuke et al. performed photodissociation experiments and ab initio calculations on $Mg^+(H_2O)_n$ ($n = 1-5$) and $Ca^+(H_2O)_n$ ($n = 1-6$).[24] Both evaporation products $Mg^+(H_2O)_{n-1}$ and reaction products $Mg^+OH(H_2O)_{n-1}$ were observed upon photodissociation of $Mg^+(H_2O)_n$. The branching ratio of the two processes depended strongly on the photolysis wavelength as well as the number of solvent molecules. The researchers observed reaction products only for $n \leq 3$, and they

* Corresponding author. E-mail address: chsyang@ust.hk.

10.1021/jp0009296 CCC: $19.00
Published on Web 08/26/2000

suggest that additional solvent molecules enhance the internal conversion rate, leading to evaporation.

In the present work, we study the photoinduced reactions in cationic complexes $M^+(AH)$, where M is an alkaline metal atom and AH is an alkyl halide molecule. This endeavor is in parallel with recent interest in the reactions of sodium with halogen-containing molecules.[7] We identified photoinduced reaction products and measured relative product yields as a function of the excitation wavelength for several metal cation−alkyl halide complexes. Quantum ab initio calculations were carried out for both the ground state and relevant excited-state potential energy surfaces in order to understand the dynamic processes. Preliminary results on the photodissociation of Mg^+-FCH_3 have been reported earlier.[25] In the following, we describe our experimental and calculational methods, present the results, and discuss the implications. Finally, we conclude our studies on the photoinduced reactions of the title complexes.

II. Experimental Section

The main experimental setup has been described previously.[26] Only the part relevant to the present experiment is given here. The metal cation−molecule complexes Mg^+-XCH_3 (X = F,Cl) were produced in a pickup ion source, which consists of a pulsed nozzle and a laser-ablation setup. A rotating magnesium disk (1.3 cm in diameter) was mounted 15 mm downstream from the exit of the pulsed valve. The sample disk rotation allowed fresh spots to be exposed to the ablation laser beam so as to produce uniform intensities of the desired complex ions. The XCH_3 gas seeded in argon (XCH_3/Ar ~ 20%) expanded supersonically through a 0.5 mm diameter orifice of the pulsed valve (R. M. Jordan) operated at a backing pressure of ~40 psi. This generated a pulse of XCH_3 gas with a duration of ~60 μs. The laser beam of the second harmonic (532 nm) of a Nd:YAG laser (~30 mJ/pulse) was weakly focused on the sample disk with a 1 mm diameter spot size. The laser-vaporized species dominated by metal ions and atoms traveled perpendicular to the supersonic jet stream 20 mm from the ablation sample target, and were picked up by cluster species in high-density regions of the supersonic jet, forming complexes with clusters and molecules. The nascent complexes were carried by the expanding stream of the supersonic jet to the extraction region of a reflectron time-of-flight mass spectrometer (RTOFMS). A distance of 10 cm from the crossing region and 5 cm upstream from the extraction region of RTOFMS, a 2 mm diameter skimmer was located to collimate the molecular beam.

The cation−molecule complexes Mg^+-XCH_3 were accelerated vertically by a high voltage pulse (1120 V in amplitude and 25 μs in width) in a two-stage extractor of the RTOFMS. After extraction, the cation−molecule complexes were steered by a pair of horizontal plates and a pair of vertical deflection plates in sequence, and then mass-selected with a pulsed high-voltage deflection plate assembly in the middle of the flight tube. Photodissociation took place in the ion turn-around region of the reflectron assembly, where the kinetic energy of parent ions was close to zero.[14] After photodissociation, the parent and fragment ions were accelerated again by the reflectron electric field and mass analyzed on the basis of their flight time through the second field-free region of the RTOFMS. The dissociation laser was a pulsed tunable dye laser pumped by an XeCl excimer laser (Lambda Physik LPX210i/LPD3002). The intensities of all the photofragment ions were recorded as the laser wavelength was scanned to obtain the photodissociation action spectrum. The dissociation laser fluence was kept low (<1 mJ/cm^2), and the dependence of fragment ion intensities on the laser fluence was monitored to ensure that the photoinduced processes of the cation−molecule complexes are in the one-photon regime.

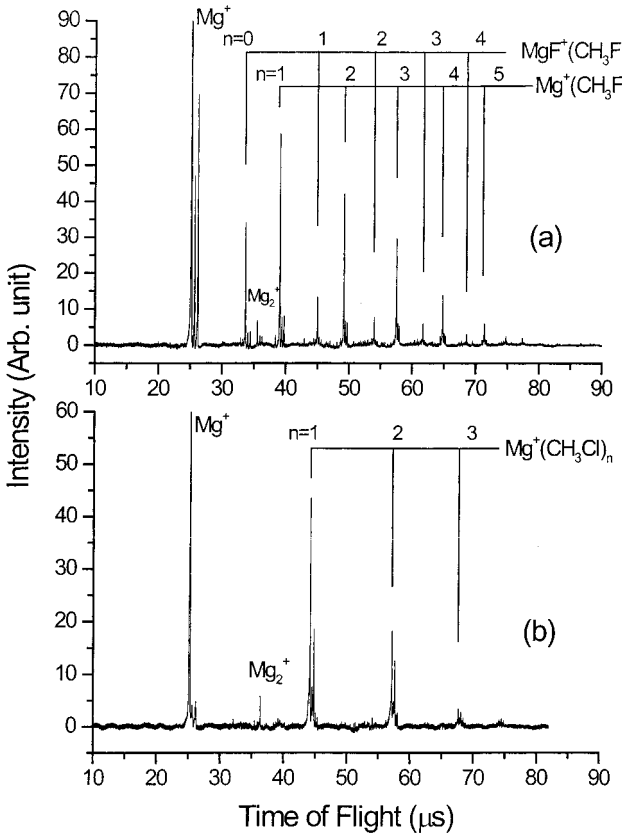

Figure 1. Time-of-flight mass spectra of the $Mg^+ + CH_3F$ system (a) and the $Mg^+ + CH_3Cl$ system (b).

III. Results and Discussion

A. Formation of Cation−Molecule Complexes. Typical mass spectra of the cationic species from the pickup source are displayed in Figure 1. The metal-bearing mass peaks can be easily recognized from the characteristic isotope distribution of magnesium (^{24}Mg, 78.99%; ^{25}Mg, 10.00%; ^{26}Mg, 11.01%).[27] As shown in Figure 1a for the $Mg^+ + FCH_3$ system, two series of mass peaks can be identified. The series of higher intensity is assigned to the cation-cluster complexes $Mg^+-(FCH_3)_n$, and the other of lower intensity to the reaction products $MgF^+-(FCH_3)_n$. We put the positive charge on Mg and MgF in the formula of these clusters because the ionization potentials of the Mg atom (7.646 eV) and MgF (8.1 eV) are much lower than that of FCH_3 (12.47 eV).[27,28] For the $Mg^+ + ClCH_3$ system, the mass spectrum is shown in Figure 1b. Unlike the $Mg^+ + FCH_3$ system, only the association complex series $Mg^+-(ClCH_3)_n$ shows up for the $Mg^+ + ClCH_3$ system with a negligible signal intensity of reaction products. This can be explained by the difference in the enthalpy of the reaction between the two systems. Although the reactions of both systems are endothermic, the reaction ($ClCH_3 + Mg^+ \rightarrow MgCl^+ + CH_3$) is endothermic by 0.6 eV, whereas the reaction ($FCH_3 + Mg^+ \rightarrow MgF^+ + CH_3$) is endothermic by only 0.4 eV.[27,28] Therefore, the former reaction is likely to have a higher activation energy than the latter reaction.

We also examined mass spectra of the systems $Ca^+ + XCH_3$ (X = F, Cl). Only very weak signals of the complexes Ca^+-XCH_3 were observed, and the mass spectra were dominated by the thermal reaction products $CaX^+-(XCH_3)_n$. It appears that

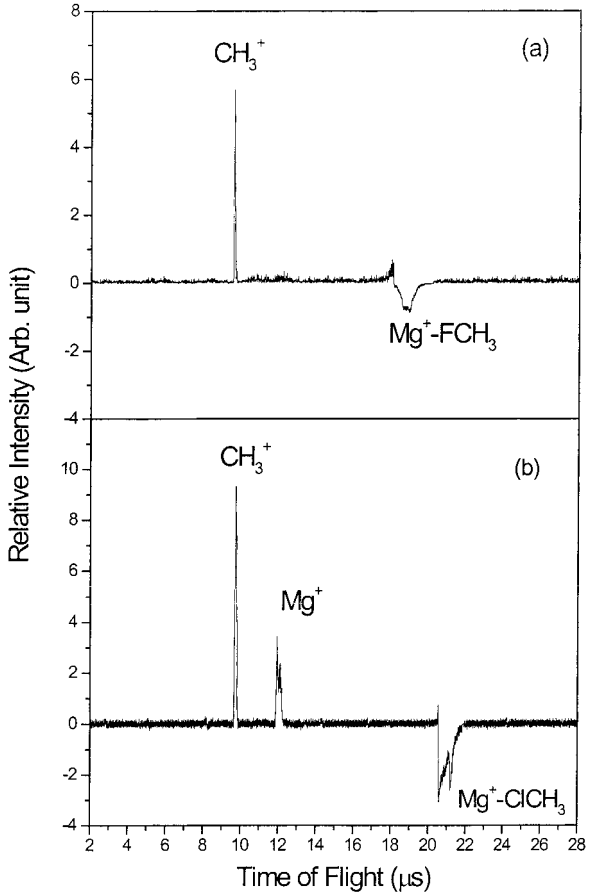

Figure 2. The photodissociation difference mass spectra for (a) Mg^+-FCH_3 at 320 nm, and (b) Mg^+-ClCH_3 at 260 nm.

the relative abundance of $M^+-(XCH_3)_n$ and $MX^+-(XCH_3)_n$ in the pickup source is determined by the binding energies and reactivities of alkyl halides XCH_3 with the metal cations Mg^+ and Ca^+. In both mass spectra of Figure 1, parts a and b, the $Mg^+-XCH_3)_{n>1}$ cluster species are obviously the association products from collisions between Mg^+ and $(XCH_3)_n$, which were produced by the pulsed supersonic nozzle. These cation−molecule complexes could be stabilized by either a third-body collision or by evaporation of an alkyl halide molecule XCH_3 from $(XCH_3)_n$. Their intensities could be controlled by adjusting the concentration of XCH_3 in the argon carrier gas and the pulse width of the pulsed valve. In this work, we focus on photoinduced reactions of the simple binary cation−molecule complexes Mg^+-XCH_3 (X = F, Cl). Therefore, the source conditions were chosen to minimized the formation of large clusters and enhance the yield of the binary complexes Mg^+-XCH_3. It was found that low concentration of XCH_3 and short gas-pulse duration is favorable to the formation of the binary complexes.

B. Photodissociation of Mass-Selected Cation−Molecule Complexes. Figure 2 presents photodissociation difference mass spectra recorded after the mass-selected parents Mg^+-FCH_3 and Mg^+-ClCH_3 were excited by the laser light at 320 and 260 nm, respectively. The negative-going peak on the high mass side signifies a depletion of the mass-selected parent due to photofragmentation, and the positive-going peaks indicate the appearance of daughter ions from photofragmentation of the parents. The relatively poor mass resolution for the negative-going parent peaks is due to the fact that the extractor and reflectron voltage settings were all optimized for the maximum overlap between the photolysis laser beam and the mass-selected parent ion packet in the ion-turn-around region of the reflectron assembly. The better mass resolution of the daughter ion peaks can be ascribed to the small size of the photolysis laser beam (5 mm diameter) and the reduced kinetic energies of the daughter ions.

The most striking difference between the two photodissociation difference mass spectra shown in Figure 2 is that while two dissociation product ions (CH_3^+ and Mg^+) are produced from Mg^+-ClCH_3 (Figure 2b), only a single dissociation product ion CH_3^+ is observed in the photolysis of Mg^+-FCH_3 (Figure 2a). The relative yields of the above two photodissociation products reflect the competition between a photoinduced reaction channel (formation of CH_3^+) and a nonreactive quenching pathway (breakup of the cation−molecule complex) of the photoexcited complex $[Mg^+-XCH_3]^*$. Even in the case of Mg^+-ClCH_3, the Mg^+ daughter ion signal is much weaker, and the dominant photodissociation channel is still the formation of CH_3^+. This is remarkable in the sense that this dominant photodissociation channel is not particularly favored by the energetics of the reactions in comparison with other channels. For example, $\Delta E = +3.3$ eV for the reaction channel ($Mg^+-FCH_3 \rightarrow CH_3^+ + MgF$), whereas $\Delta E = +1.6$ eV for ($Mg^+-FCH_3 \rightarrow CH_3 + MgF^+$).[27,28] In fact, as described above, only the product series $MgF^+(FCH_3)_n$ (instead of $CH_3^+(FCH_3)_n$) was observed in the thermal reaction of the pickup source. In addition, the photodissociation pattern is also in contrast to the results of previous photodissociation experiments on other cation−molecule binary complexes such as Mg^+-CH_3OH.[29] In the photodissociation of Mg^+-CH_3OH, Mg^+ was found to be the most prominent fragment from photodissociation of cation−molecule complexes. The fragment CH_3^+ was observed with a very low intensity compared with those of the dominant photofragments Mg^+ and $MgOH^+$. An interesting charge-transfer photodissociation pattern in metal cationic complexes was first reported by Duncan et al.[30] and later extended to other systems by Kleiber et al.[31] However, this type of reaction is still quite different from the present reaction in question, which involves both atom extraction and charge-transfer. We believe that the dominant photoinduced reaction channel we identified results from severe kinetic constraints and involves curve-crossing from initial vertical excitation to an exit potential energy surface, leading to the formation of metal halide and CH_3^+. A more detailed mechanism of this photoinduced reaction will be discussed in the following parts of this section.

Photodissociation action spectra were taken by monitoring product ion signals (Mg^+ and CH_3^+) when the dissociation laser wavelength was scanned. In taking the photodissociation action spectra, the dissociation laser fluence was kept low (<1 mJ/cm^2) so as to minimize the multiphoton processes. Moreover, both the fragment ion and parent ion intensities and the dissociation laser fluence were recorded for normalization of the photodissociation action spectra. An examination on the laser fluence dependence of the fragment ion intensities showed a one-photon process. All the photodissociation action spectra were taken in this one-photon regime.

The photodissociation action spectra of the Mg^+-XCH_3 (X = F, Cl) complexes in the wavelength range of 230−390 nm are given in Figure 3. The daughter ion signal intensity was normalized against both the parent ion signal intensity and the dissociation laser fluence. The spectra were collected in segments and the different segments were pieced together by normalizing the spectra at the overlapping edges of the laser dye ranges. There are two pronounced peaks in the photodissociation action spectrum of Mg^+-FCH_3 shown in Figure 3a.

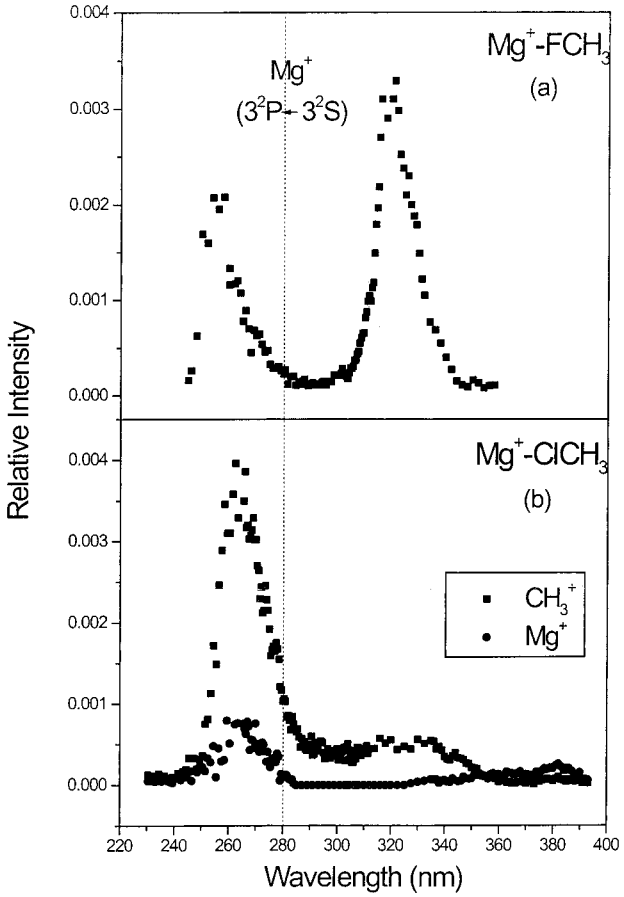

Figure 3. Photodissociation action spectra of (a) Mg^+-FCH_3, and (b) Mg^+-ClCH_3. The wavelength of the Mg^+ ($3^2P \leftarrow 3^2S$) atomic transition is shown by a dotted line.

These two peaks are centered at around 255 and 320 nm, which are at the blue side and red side of the Mg^+ ($3^2P \leftarrow 3^2S$) atomic transition, respectively. For the photodissociation of Mg^+-ClCH_3 (Figure 3b), both the reactive CH_3^+ channel and nonreactive channel Mg^+ are open, and the corresponding action spectra are quite different. Overall, the action spectra show two peaks with different intensity ratios on both sides of the atomic transition of Mg^+ ($3^2P \leftarrow 3^2S$). While the photodepletion action spectra of $Na-XCH_3$ are similar for different X,[7e] the action spectrum of Mg^+-ClCH_3 is quite different from that of Mg^+-FCH_3. For example, two peaks of comparable intensity were observed in the photodissociation action spectrum of Mg^+-FCH_3, whereas for the reactive channel (CH_3^+) of $[Mg^+-ClCH_3]^*$, only one pronounced peak centered at ~265 nm is observed and adjacent to it is a broad but weak bump in the wavelength range of 300−350 nm. On the other hand, the intensity of the nonreactive channel product ion Mg^+ is much lower than that of CH_3^+ in nearly all the spectral regions of the recorded action spectrum except in the range of 360−390 nm. The peak assignments of these action spectra will be discussed based on available data from literature and ab initio calculations in the following subsections.

C. Theoretical Calculations. Bauschlicher's group performed extensive ab initio calculations on alkaline earth metal cation−solvent complexes in both the ground state and excited states.[32] Their results were demonstrated to be quite accurate by some experimental works.[12,17] Polanyi et al. also conducted ab initio calculations on potential energy surfaces of both the ground and excited states of $Na-XCH_3$ (X = F, Cl, Br),[7e] and the results were found to agree well with their photodepletion action spectra of these systems.

In our calculations, the ground-state geometry for the systems Mg^+-XCH_3 was fully optimized at the second-order Moller−Plesset (MP2) level by using the GAUSSIAN 98 package. The basis set of 6-31+G** was used in the present work. The binding energy of a given cation−molecule complex Mg^+-XCH_3 is defined as the difference between the total energy of Mg^+-XCH_3 in its optimized ground-state geometry, $E(Mg^+-XCH_3)$, and the total energies of isolated Mg^+ and XCH_3 in the gas phase, $E(Mg^+) + E(XCH_3)$. The superposition error was calculated to be 8×10^{-3} kcal/mol for X = F. This is insignificant compared with the complex binding energy and was therefore neglected. For the potential energy surfaces of the complex excited states, we used a less extended CI referred to as the CI-single (CIS) approach. Obviously, these calculations are not quantitatively accurate especially at points of configuration space where electronic degeneracy exists. Nevertheless, in the present work, what we aim at is a qualitative interpretation of our action spectra. The binding energy for a given excited state of a cation−molecule complex is defined as the difference between the energy of Mg^+-CH_3 in the excited state and the sum of energies of the free Mg^+ in the 3^2P state and XCH_3 in its ground state.

As a starting structure for calculation, we tried to attach the alkaline earth metal ion to the XCH_3 molecule from both the X and CH_3 ends. However, the minimum-energy structures were found to be always those in which the cation Mg^+ points to the X end with an overall C_s symmetry. This is consistent with the observed photoinduced reaction channel, which yields CH_3^+ and MgX as the products. Similar results were also obtained for $Na-FCH_3$ by Polanyi et al.; their calculations showed that the minimum-energy structures for alkaline earth metal cation or alkali metal atom plus a solvent molecule have the negatively charged end of the solvent molecule (such as X in XCH_3) pointing toward the metal cations or atoms. Table 1 lists some calculated structural parameters of the cation−molecule complexes in the ground and first three excited states. The structural parameters include bond lengths, bending angles, and binding energies for the minimum energy structures. Structural differences between cation−molecule complexes Mg^+-FCH_3 and Mg^+-ClCH_3 emerge clearly from Table 1. Notably, the bending angle θ of Mg^+-FCH_3 (179.7°) is much larger than that of Mg^+-ClCH_3 (113°). For the ground state $(1)^2A'$, the complex Mg^+-FCH_3 has a higher binding energy than that of Mg^+-ClCH_3, i.e., the ground state of Mg^+-FCH_3 is more strongly bound than the ground state of Mg^+-ClCH_3. This bond strength trend is also reflected in the bond lengths of these two complexes. Due to the relatively strong cation−molecule interaction, the X−C bond is apparently stretched compared with the bond length in gas-phase XCH_3 molecules. This has the effect of bringing the complex structure even closer to the transition state configurations, and is in this sense beneficial to transition state spectroscopy.

The Mg−X bond distances for the $(2)^2A'$ and $(1)^2A''$ states of both complexes are shorter than those in the $(1)^2A'$ ground state. This results from the reduced Mg^+ 3s-ligand repulsion by promoting the 3s electron into 3p orbitals, two of which are perpendicular to the Mg-X bond axis. This reduction in metal−ligand repulsion also results in larger binding energies for the excited states of the complexes with respect to their asymptotes. On the other hand, the $(3)^2A'$ states have smaller binding energies than those of the ground states of both complexes. This can be explained by noticing the increased metal−ligand

TABLE 1: Summary of the Main Results from the ab Initio Calculations for the Ground and the First Three Excited States of Mg^+-FCH_3 and Mg^+-ClCH_3

	Mg^+-CH_3					Mg^+-ClCH_3			
electronic state	r_{Mg-F}(Å)	r_{F-C}(Å)	θ (deg)	D_0 (kcal/mol)	electronic state	r_{Mg-F}(Å)	r_{F-C}(Å)	θ (deg)	D_0 (kcal/mol)
$(1)^2A'$	2.007	1.488 (1.382)[a]	179.7	26.8	$(1)^2A'$	2.546	1.816 (1.785)[a]	113.5	20.2
$(2)^2A'$	1.924	1.445	152.3	44.3	$(2)^2A'$	2.357	1.858	116.0	47.7
$(1)^2A''$	1.918	1.445	177.2	43.4	$(1)^2A''$	2.425	1.849	113.1	40.9
$(3)^2A'$	1.952	1.502	179.6	13.5	$(3)^2A'$	3.472	1.823	179.5	20.0

[a] r_{X-C} of the gas-phase methyl halide XCH_3.[27]

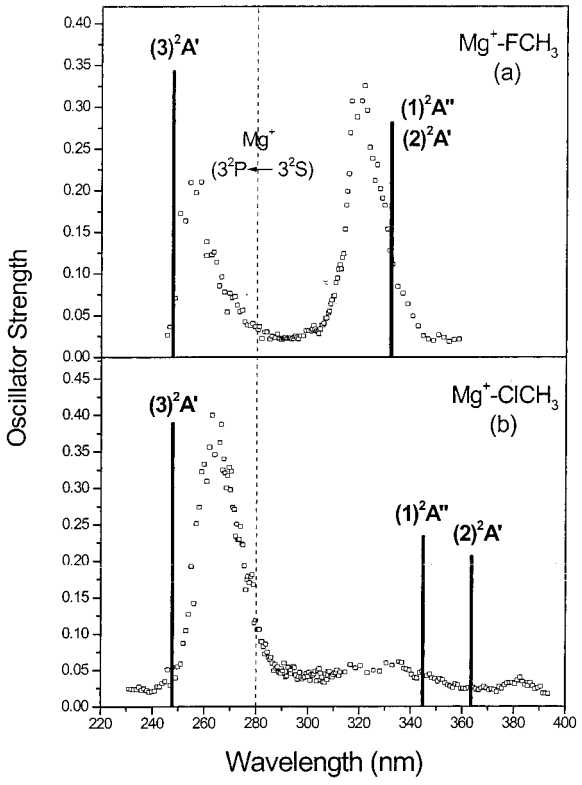

Figure 4. Calculated excitation spectra of Mg^+-FCH_3 (a) and Mg^+-ClCH_3 (b) at their minimum-energy structures. The position and length of the solid lines indicate the calculated transition energies and the corresponding oscillator strengths. The broken line shows the position of the Mg^+ ($3^2P \leftarrow 3^2S$) atomic transition. Experimental integral action spectra are re-plotted here for comparison. Note that the overlapping transitions to $(1)^2A''$ and $(2)^2A'$ in (a) have nearly the same oscillator strength according to the calculation.

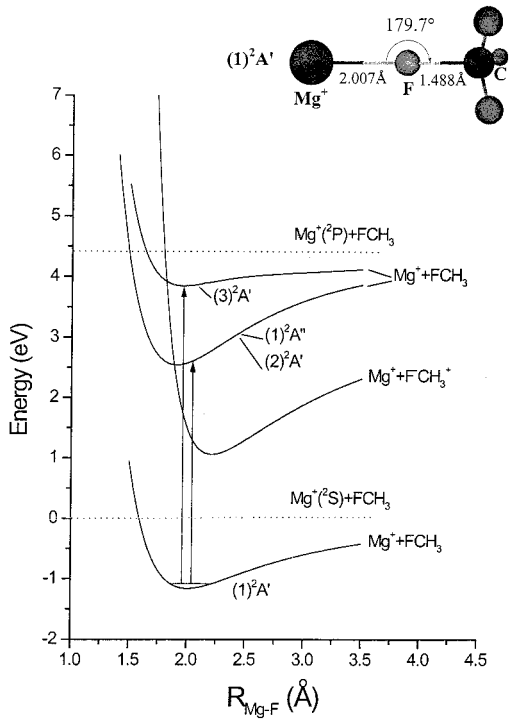

Figure 5. Qualitative potential energy curves for the Mg^+-FCH_3 system along the coordinate of the Mg−F bond distance. The ground state and the first three excited PESs are calculated from the ab inito calculations. The ionic curve is schematically constructed on the basis of relevant known physical parameters. The ground-state structure of Mg^+-FCH_3 is also shown.

repulsion when the 3s electron is promoted to the 3p orbital which aligns along the Mg^+-X bond axis.

D. Peak Assignments of the Action Spectra. On the basis of the above ab initio results, vertical excitation energies to the first three excited states of Mg^+-FCH_3 and Mg^+-ClCH_3 were calculated using an optimized geometry for their ground states. The results are graphically shown in Figure 5. The solid lines constitute the excitation spectra of the complexes, with their locations representing the excitation energies and amplitudes representing the oscillator strengths of the transitions. The broken line indicates the Mg^+ ($3^2P \leftarrow 3^2S$) atomic transition. As has been discussed above, the cation−molecule interaction between Mg^+ and XCH_3 splits the 3^2P excited state of Mg^+ into three sublevels, and the magnitude of the splitting depends on the orientations of the three $3p_{x,y,z}$ orbitals with respect to the Mg^+-X bond axis. For the two excited states $(2)^2A'$ and $(1)^2A''$, one of the two $3p_{x,y}$ orbitals of Mg^+ perpendicular to the Mg^+-X bond axis is occupied by an electron excited from the 3s orbital. On the other hand, the $3p_z$ orbital oriented along the Mg^+-X bond axis is occupied by an excited electron in the excited state $(3)^2A'$. The energies of $(2)^2A'$ and $(1)^2A''$ are lowered owing to the reduced electron density in the direction of the Mg^+-X bond axis, whereas the excited state $(3)^2A'$ becomes higher in energy due to the direct repulsive interaction between the parallel $3p_z$ electron of Mg^+ and the nonbonding electrons of X. A further splitting between the $(2)^2A'$ and $(1)^2A''$ states is induced by the CH_3 umbrella in a bent configuration. According to our calculational results tabulated in Table 1, the Mg^+-F-C angle of the minimum energy structure of the ground-state Mg^+-FCH_3 is nearly 180°, so the $(2)^2A'$ and $(1)^2A''$ states are almost degenerate, and therefore cannot be distinguished in Figure 4a. In contrast, the Mg^+-Cl-C angle of the minimum energy structure of the ground-state Mg^+-ClCH_3 113.5°, which is close to a perpendicular geometry. As a result, the degeneracy of $(2)^2A'$ and $(1)^2A''$ states is lifted, and two corresponding peaks appear in Figure 4b.

With the available data from literature and the results from the above calculations, we are in the position to make assignments of the photodissociation action spectra in Figure 3. In the action spectrum (the CH_3^+ yield) of Mg^+-FCH_3 shown in

TABLE 2: Some Relevant Physical Parameters Useful for the Energetics of Mg^+-XCH_3 (X = F, Cl) Photodissociation

bond	BE (eV)		IP (eV)		EA (eV)
Mg−F	4.75[a]	Mg	7.646[a]	F	3.4[a]
Mg−Cl	3.3[a]	CH_3	9.83[a]	Cl	3.61[a]
CH_3−F	4.7[a]	CH_3F	12.47[a]	CH_3F	−6.2[e]
CH_3−Cl	3.5[a]	CH_3Cl	11.22[a]	CH_3Cl	−3.45[e]
Mg^+−F	4.3[b]	MgF	8.1[d] (7.7)[b]		
Mg^+−Cl	2.87[b]	MgCl	8.1[d]		
Mg^+−F	8.9[c]				
Mg^+-Cl^-	7.3[c]				

[a] Taken from ref 27. [b] Our ab initio calculation results. [c] Calculated from the BE of Mg−X bond, IP of Mg atom, and the EA of X atoms. [d] Calculated from the BE of Mg−X, Mg^+−X, and the IP of Mg atom. [e] Taken from ref 34.

Figure 3a, the peak centered at ∼320 nm is ascribed to a superposition of the excitations to the $(2)^2A'$ and $(1)^2A''$ states because these two states are quite close in energy. The remaining peak centered at ∼255 nm is then assigned to the transition to the $(3)^2A'$ state. The action spectra of Mg^+-ClCH_3 are more complicated as seen in Figure 3b. The only pronounced peak centered at ∼265 nm for both product channels CH_3^+ and Mg^+ can be easily assigned to the transition to the $(3)^2A'$ state of Mg^+-ClCH_3. The position of this peak is closer to the Mg^+ ($3^2P \leftarrow 3^2S$) atomic transition than that of Mg^+-FCH_3, and this can be explained by noticing that the well depth of the $(3)^2A'$ state for Mg^+-ClCH_3 is of a magnitude similar to that of its ground-state according to our calculation. At the calculated positions corresponding to excitations to the $(2)^2A'$ and $(1)^2A''$ states, no intense peak is present except two weak bumps in the wavelength ranges of 300−350 nm and 360−390 nm for the reactive (CH_3^+) and nonreactive (Mg^+) channels, respectively.On the basis of results from our calculation (Figure 4b), we assign one of the small bumps on the blue side (CH_3^+ channel) to the transition to the $(1)^2A''$ state and the other on the red side (Mg^+ channel) to the transition to the $(2)^2A'$ state.

It should be pointed out that the peak height in Figure 3 is associated with the photodissociation yield of a specific fragment ion. This yield depends not only on the oscillator strength of the transition to the excited state but also the probability for the excited state to find its way to the exit channel, in which the fragment ion emerges. In this sense, the amplitudes of the peaks in the action spectra (Figure 3) may be quite different from the oscillator strength distributions shown in Figure 4. However, compared with the calculated oscillator strengths from ground state to the excited states of Mg^+-FCH_3 shown in Figure 4a, the integrated peak intensities in the observed action spectrum show satisfactory agreement (Expt: $I_{blue}:I_{red} = 1:1.60$; Calcd: $I_{blue}:I_{red} = 1:1.65$). The relatively high intensity of the peak on the red side can be explained by the superposition of the transitions to the lowest two excited states. We therefore conclude tentatively that the reactivities of the three excited states of Mg^+-FCH_3 are similar. This does not seem to be the case for Mg^+-ClCH_3. According to the comparison of Figure 3b,c, the three excited states of Mg^+-ClCH_3 appear to possess different reactivities and with different branching ratios of the reaction channel to the quenching channel (Expt: $I_{blue}:I_{middle}:I_{red} = 1:0.17:0.05$; Calcd: $I_{blue}:I_{middle}:I_{red} = 1:0.59:0.54$). Further discussions on the photofragmentation mechanism will be given below.

E. Dynamics of the Photoinduced Reaction and Nonreactive Quenching. At this point, one may still cast doubt about the structural entity of Mg^+-XCH_3. Although the formation of $MgX(CH_3^+)$ is endothermic by almost 2 eV (Table 2), it might be possible to form $MgX^+(CH_3)$ in the pickup source.

TABLE 3: Charge Distributions with Hydrogens Summed into Heavy Atoms from the ab Initio Calculation for the Ground and the First Three Excited States of Mg^+-FCH_3 and Mg^+-ClCH_3

electronic state	Mg^+-FCH_3			electronic state	Mg^+-ClCH_3		
	Mg	F	C		Mg	Cl	C
$(1)^2A'$	0.86	−0.42	0.56	$(1)^2A'$	0.66	0.09	0.25
$(2)^2A'$	0.85	−0.37	0.52	$(2)^2A'$	0.55	0.15	0.30
$(1)^2A''$	0.86	−0.40	0.53	$(1)^2A''$	0.59	0.13	0.28
$(3)^2A'$	0.85	−0.43	0.57	$(3)^2A'$	0.95	−0.15	0.20

However, this is contrary to our findings so far. First, the species $MgX^+(CH_3)$, if present, must come from the recombination of the thermal reaction products MgX^+ and CH_3. In this situation, the abundance of MgX^+ should be much higher than that of $MgX^+(CH_3)$, which contradicts the mass spectral observation (Figure 1). Second, the action spectra (Figure 3) show clearly that the peaks between the atomic transition Mg^+ ($3^2P \leftarrow 3^2S$) are derived from the excitations centered at Mg^+, but perturbed significantly by the presence of XCH_3. On the other hand, MgX^+ is a closed shell species in $MgX^+(CH_3)$, and therefore the excitation spectra of $MgX^+(CH_3)$ must originate from CH_3, which should be qualitatively different from the spectra we observed. Finally, the results from our ab initio calculations at the MP2 level suggest that the ground-state minimum energy structure of the complex should be Mg^+-XCH_3 with the X−C bonds slightly extended relative to those of the free XCH_3. (Table 1). It is perhaps more clear from Table 3, that the Mg in both complexes carries only a fraction of unit positive charge, whereas in MgX^+, Mg should carry two units of positive charge.

Another concern is related to the pickup source we used. This pickup source might produce hot complexes, which for one thing would cause possible ground-state reactions, and second, broaden the spectral peaks as shown in Figure 3. The first possibility entails intra-cluster conversion from Mg^+-XCH_3) to $MgX^+(CH_3)$. Because this conversion has to surmount a substantial barrier, the probability is expected to be small. In addition, if the conversion is significant, we should expect a substantial temperature dependence of the action spectra. To clarify this issue, we checked the action spectrum of Mg^+-FCH_3 produced using a nozzle source in a certain wavelength range with a sufficiently short scanning step. The action spectrum taken using the nozzle source and that using the pickup source are quite similar. Therefore, most complexes in the pickup source should have the form Mg^+-XCH_3. Although the envelope is sharpened to a certain extent due to the use of the colder nozzle source, no fine features have been identified. We notice that Farrar and co-workers obtained much better resolved spectra of Sr^+H_2O/Sr^+D_2O using a nozzle source than those using a pickup source.[21] In this sense, our failure in obtaining well-resolved action spectra of Mg^+-FCH_3 may be due to the rapidity of the photoinduced reactions. Further work will be carried out on this issue. We also measured the photodissociation spectrum of Mg^+-OCO from the pickup source, which was first recorded by Duncan et al. and which possesses well-defined vibrational structures.[23] Although we obtained a vibrationally resolved photodissociation spectrum for Mg^+-OCO, the line widths indicate that the complex ions from our pickup source is still much hotter than those seen by other workers. Clearly, the complex temperature can be significantly lowered using the nozzle source. Future experiments are planned to improve our nozzle source and take the action spectra of truly cold complexes. This would clarify the role of temperature in the action spectra of the complexes.

Having addressed the identity of the parent complexes, we now consider the dynamics of these complexes upon photoex-

citation. Before doing this, we want to point out that the opening of the reaction channels is energetically possible for all the 3^2P states of both complexes according to the data in Tables 1 and 2. As mentioned above, experiments also suggest one-photon dissociation processes for all the wavelengths we employed in this study. There are several possible relaxation pathways following the photoexcitation of a metal cation−molecule complex to an excited-state centered on Mg^+ ($3p \leftarrow 3s$). First, internal conversion may occur, leading to the cleavage of the cation−molecule bond. Second, the excited complex may make a radiative transition back to the ground state. The most interesting scenario involves curve-crossing from the potential energy surface (PES), prepared by the optical excitation, to a reactive PES which intersects the initial PES at a specific nuclear configuration; such a PES crossing appears to yield inevitably the reactive product, CH_3^+ in the present case. In previous studies on the photoinduced reaction in van der Waals complexes between alkali metal atoms and alkyl halides, e.g., Na−XCH_3, a celebrated harpooning reaction mechanism was proposed, which embodies an electron-transfer step from the metal atom M to the halide RX upon excitation.[7e] The electron-transfer results in the formation of RX^-, and because the negatively charged halide molecule is unstable, it dissociates to X^-, which joins M^+ to form M^+X^-. The photoinduced reaction we observed in Mg^+-FCH_3 and Mg^+-ClCH_3 seems to originate also from a charge-transfer mechanism. However, it is not possible for an electron to jump from the metal atom to the halide due to the extremely high ionization potential of Mg^+ (15.035 eV) and the large negative electron affinity of XCH_3 (Table 2). On the other hand, it is also difficult for an electron to transfer from XCH_3 to the excited $(Mg^+)^*$.

What is actually happening may be a concerted action of the two processes mentioned above although an individual process of the two is unlikely to occur. Specifically, when the outermost 3s electron of Mg^+ is excited to 3p, it attains a sufficient energy to transfer gradually to the halide molecules $X-CH_3$, rendering the X−C bond to extend. As the X−C bond becomes longer and longer, the electron in XCH_3 is more and more easily ionized because CH_3 has a much lower ionization potential than XCH_3. Therefore, the electron also transfers gradually from XCH_3 to Mg^+, and this in turn would facilitate the electron transfer from Mg^+ 3p to XCH_3. The concerted process described above would result in an intermediate $[Mg^+-X^--CH_3^+]$, in which the X−C bond is much extended. Before MgX finds itself having a lower ionization potential than that of CH_3, the CH_3^+ moiety is already released from the molecular field of MgX. Therefore, the final outcome of the reaction would be the formation of MgX and CH_3^+ instead of MgX^+ and CH_3. The striking photoinduced reaction pattern in Mg^+-FCH_3 and Mg^+-ClCH_3 appears to result from the peculiar topology of the excited-state potential energy surfaces, which places severe kinetic constraints on the exit channels. The consequence of these kinetic constraints is the formation of a photoproduct, which is energetically unfavorable.

The scenario described above can be better illustrated in terms of the relevant potential energy surfaces. In an effort to determine the possible dissociation and reaction pathways, we carried out a series of potential energy scans of the ground and first three excited states of cation−molecule complexes Mg^+-XCH_3 (X = F, Cl) using GAUSSIAN 98. The method of our calculation and the basis set we used are the same as we have described above. Considering the vertical excitation, the excited state geometry used in the calculation is the optimized geometry for the ground state. While the level of the calculation for the excited states is not sufficiently accurate to obtain reliable quantitative information about the absolute energies, the qualitative nature of the potential energy surfaces should be correct. The diabatic potential energy surfaces of the ground and three excited states for Mg^+-FCH_3 and Mg^+-ClCH_3 from the PES scans are shown in Figures 5 and 6, respectively, along the coordinate of the Mg−X bond distance. In Figure 5, the PES of the excited state $(2)^2A'$ of the complex Mg^+-FCH_3 overlaps with that of $(1)^2A''$. Since the photoinduced reaction must involve a crossing from diabatic covalent curves to diabatic ionic curves to find its way to the final products, we have also schematically shown PESs involving possible asymptotic ionic species ($Mg^+ + X^-CH_3^+$ and $Mg^+X^- + CH_3^+$ in this case because CH_3^+ is the dominant reaction product) in Figures 5 and 6. We have used parameters of the relevant asymptotes from the literature and from our calculations in constructing these PESs.[7d,28,33] The relative energy levels of the possible ionic products $Mg^+X^- + CH_3^+$ were determined from the bond dissociation energies of CH_3-X and Mg−X; electron affinities of the X atoms (X = F, Cl) and the ionization potentials of the Mg atom and CH_3, which are all listed in Table 2.

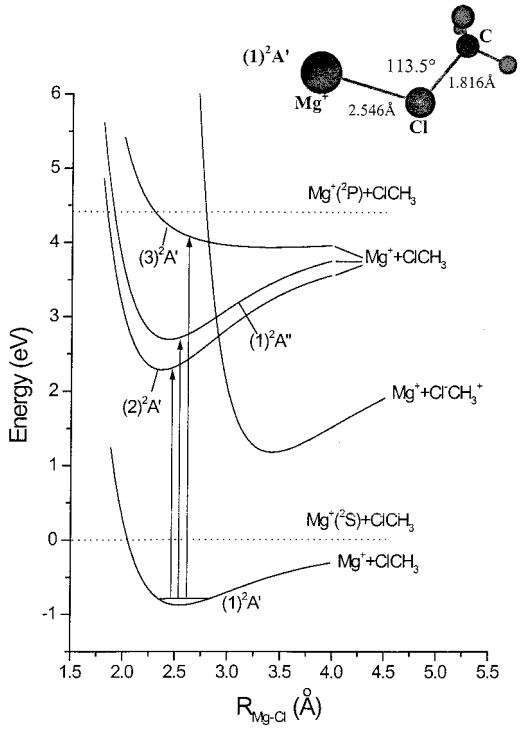

Figure 6. Qualitative potential energy curves for the Mg^+-ClCH_3 system along the coordinate of the Mg−Cl bond distance. The ground state and the first three excited PESs are calculated from the ab inito calculations. The ionic curve is schematically constructed on the basis of relevant known physical parameters. The ground-state structure of Mg^+-ClCH_3 is also shown.

For the Mg^+-FCH_3 system in Figure 5, the excited-state potential energy curves must cross some sort of ionic potential energy curve at certain point of configuration space, where the electronic excitation energy can be converted to the energy of nuclear motion, driving the reaction to completion in the ground state. Considering the fact that the final products are MgF and CH_3^+, the reaction mechanism is likely to involve the ionic species $F^-CH_3^+$. The ionic potential curve is then associated with the asymptote ($Mg^+ + F^- + CH_3^+$). As can be seen in Figure 5, the ionic ($Mg^+ + F^- + CH_3^+$) curve crosses the excited PES near the bottom of the potential wells. Upon excitation to these states, the cation−molecule complex has a ready access to the crossing points, where it switches from the

initial PES to the ionic PES, sliding down the steep ionic curve to form the product $MgF + CH_3^+$. The trajectory is likely to be downhill along the coordinate of the F−C bond distance of $[Mg^+-F^--CH_3^+]^*$. On the contrary, the crossing points between the excited PESs and the ground-state $Mg^+ + F- - -CH_3$ curve are at a much higher energy, and therefore it is unlikely for the excited states of the complex to relax directly to the ground state through curve crossing. This explains why the products $Mg^+ + FCH_3$ were not observed. One possibility is that the excited complex may be trapped and it would undergo radiative decay to continuum levels of the ground-state surface. But the radiative lifetime of the excited intermediate complex would probably be close to that of the bare Mg^+ chromophore in the excited states 3^2P, ~3 ns,[27] and it seems unlikely that any reaction mechanism would have such a slow rate. Therefore, the reaction toward $MgF + CH_3^+$ is left as the only photodissociation channel for the cation−molecule complex Mg^+-FCH_3. Consequently, once excited, the complex will turn into the products CH_3^+ and MgF. In this sense, the three excited states of Mg^+-FCH_3 would show similar reactivities as mentioned above.

The photodissociation action spectra of Mg^+-ClCH_3 are quite different from that of Mg^+-FCH_3, mainly in two aspects. First, two reaction channels are open in the relaxation of $[Mg^+-ClCH_3]^*$ including the charge-transfer reaction and the quenching process, whereas the relaxation of $[Mg^+-FCH_3]^*$ involves exclusively the charge-transfer reaction in all the wavelength regions we have studied. Second, the three excited states of Mg^+-ClCH_3 all have different reactivities as discussed above. The higher excited state $(3)^2A'$ appears to have a higher reactivity than the other two. As shown in Figure 6, the ionic PES curve ($Mg^+ + Cl^- + CH_3^+$) crosses the $(3)^2A'$ curve at a point between the Franck−Condon region and the bottom of the well. Once excited, the complex slides downhill along the Mg−Cl coordinate, and switches to the ionic curve at the crossing point, leading to the products $MgCl + CH_3^+$. However, the ionic curve crosses the $(2)^2A'$ curve at a point well above the bottom of the potential well. The excited complex $[Mg^+-ClCH_3]^*$ has to overcome a substantial barrier to reach the crossing point and therefore, it may jump radiatively back to the ground state with some probability of forming the products $Mg^+ + ClCH_3$. The $(1)^2A''$ excited-state sits between $(2)^2A'$ and $(3)^2A'$, and therefore shares the characteristics of both; it leads mainly to the reaction with a small probability of quenching. The low reactivity of $(1)^2A''$ may be related to the small probability for it to switch to the ionic curve due to the symmetry mismatch. In the quenching channel, the observed ratio of the $(1)^2A''$ state to the $(3)^2A'$ state (Figure 3b) is also smaller than that from the calculation (Figure 4b). This can be attributed to the fact that the PES bottom of $(3)^2A'$ is at a much larger Mg−Cl bond length (Figure 6); when it decays radiatively to the ground state, the complex will have a sufficient energy for dissociation. Furthermore, dissociation may also occur directly on the $(3)^2A'$ excited state surface due to the repulsive nature of this potential energy surface. In fact, photoinduced evaporation in electronically excited states of M^+-H_2O (M = alkaline metal) was established.[21,24]

One of the major differences in the photoinduced reaction dynamics between Mg^+-FCH_3 and Mg^+-ClCH_3 lies probably in the different topology of their potential energy surfaces. For example, the ground-state structure of Mg^+-FCH_3 is essentially linear (see Figure 5). In this linear configuration, the ionic curve has its energy minimum at a relatively small Mg−F bond distance. The photoexcited states in the Franck−Condon region can couple efficiently to the ionic curve (Figure 5). In contrast, Mg−Cl−C encloses an angle of 113.5° (Table 1) in the ground state of Mg^+-ClCH_3 (see Figure 6). In this configuration, the ionic curve energy minimum is located at a relatively large Mg−Cl bond distance due to the electrostatic repulsion between Mg^+ and CH_3^+. The consequence is that the $(3)^2A'$ excited state can efficiently couple to the ionic curve, whereas the coupling of the other two excited states to the ionic curves is hindered by a potential energy barrier, which is large for $(2)^2A'$ and moderate for $(1)^2A''$.

IV. Summary and Conclusions

The cation−molecule complexes $Mg^+-(XCH_3)_n$ (X = F, Cl) have been produced by using the pickup technique. Photoinduced reactions have been observed for the first time in Mg^+-FCH_3 and Mg^+-ClCH_3. Moreover, we have measured the relative photodissociation product yields as a function of the excitation wavelength in a broad spectra region. The photodissociation action spectra consist mainly of two broad peaks between the atomic transition of $Mg^+(3^2P \leftarrow 3^2S)$. Experiments on the complexes with different halide substitutions show different photoreaction patterns. In particular, photodissociation of the cationic complex Mg^+-FCH_3 produced exclusively MgF and CH_3^+, whereas more channels are open in the photodissociation of Mg^+-ClCH_3.

The photodissociation action spectra of Mg^+-XCH_3 (X = F, Cl) are discussed with the help of quantum ab initio calculations of both the ground-state and the relevant excited-state potential energy surfaces. The calculated action spectra are fairly consistent with the observed action spectra. The ratio of photodissociation peaks in the action spectrum of Mg^+-FCH_3 agrees well with the calculated oscillator strengths, whereas that of Mg^+-ClCH_3 shows difference from the corresponding calculations. This is explained by the similar reactivity of the excited states of Mg^+-FCH_3 and different reactivity of the excited states of Mg^+-ClCH_3. The different reaction patterns of Mg^+-FCH_3 and Mg^+-ClCH_3 are attributed to the different ground-state structures of the complexes, which impose the initial configurations for the excited-state reactions.

Acknowledgment. This work is supported by an RGC grant administered by the UGC of Hong Kong.

Supporting Information Available: Supporting Information Available: Three figures showing the effect of cluster sources on the photodissociation action spectra. Supporting Information is available free of charge via the Internet at http://pubs.acs.org.

References and Notes

(1) Shin, S. L.; Chen, Y.; Nicholaisen, S.; Sharpe, S. W.; Beaudet, R. A.; Wittig, C. *Adv. Photochem.* **1991**, *16*, 249.

(2) *Laser Spectroscopy and Photochemistry on Metal Surfaces*; Dai, H.-L., Ho, W., Eds.; World Scientific: Singapore, 1995.

(3) *Faraday Discuss. Chem. Soc*. **1997**, *108*.

(4) Polanyi, J. C.; Zewail, A. H. *Acc. Chem. Res*. **1995**, 28, 119.

(5) (a) Weaver, A.; Neumark, D. M. *Faraday Disscuss. Chem. Soc*. **1991**, *91*, 5; (b) Neumark, D. M. *Acc. Chem. Res*. **1993**, *26*, 33.

(6) (a) Soep, B.; Whitham, C. J.; Keller, A.; Visticot, J. P. *Faraday Discuss. Chem. Soc*. **1991**, *91*, 191. (b) Soep, B.; Abbes, S.; Keller, A.; Visticot, J. P. *J. Chem. Phys*. **1991**, *96*, 440.

(7) (a) Liu, K.; Polanyi, J. C.; Yang, S. H. *J. Chem. Phys*. **1992**, *96*, 8628. (b) ibid. **1993**, *98*, 5431. (c) Polanyi, J. C.; Wang, J. X.; Yang, S. H. *Isr. J. Chem*. **1994**, *35*, 55. (d) Polanyi, J. C.; Wang, J. X. *J. Phys. Chem*. **1995**, *99*, 13691. (e) Chang, X. Y.; Ehlich, R.; Hudson, A. J.; Polanyi, J. C.; Wang, J. X. *J. Chem. Phys*. **1997**, *106*, 3988. (f) Topaler, M. S.; Truhlar, D. G.; Chang, X. Y.; Piecuch, P.; Polanyi, J. C. *J. Chem. Phys*. **1998**, *108*, 5378.

(8) Skowronek, S.; Jimenez, J. B.; Urena, A. G. *Chem. Phys. Lett*. **1999**, *303*, 275.

(9) Loomis, R. A.; Schwartz, R. L.; Lester, M. I. *J. Chem. Phys*. **1996**, *104*, 6984.

(10) Dixon-Warren, S.; Jensen, E. T.; Polanyi, J. C.; Xu, G. Q.; Yang, S. H.; Zeng, H. C. *Faraday Discuss. Chem. Soc*. **1991**, *91*, 451.

(11) (a) Scherer, N. F.; Sipes, C.; Bernstein, R. B.; Zewail, A. H. *J. Chem. Phys*. **1990**, *92*, 5239. (b) Zewail, A. H. *Faraday Discuss. Chem. Soc*. **1991**, *91*, 207.

(12) Kleiber, P. D.; Chen, J. *Int. Rev. Phys. Chem*. **1998**, *17*, 1.

(13) Wiley, W. C.; McLaren, I. H. *Rev. Sci. Instrum*. **1955**, *26*, 1150.

(14) Cornett, D. S.; Peschke, M.; LaiHing, K.; Cheng, P. Y.; Willey, K. F.; Duncan, M. A. *Rev. Sci. Instrum*. **1992**, *63*, 2177.

(15) (a) Harris, R. M.; Herschbach, D. R. *Faraday Discuss. Chem. Soc*. **1973**, *55*, 121. (b) Neoh, S. K.; Herschbach, D. R. *J. Chem. Phys*. **1995**, *63*, 1030. (c) Kinsey, J. L.; Kwei, G. H.; Herschbach, D. R. *J. Chem. Phys*. **1976**, *64*, 2133.

(16) Moore, C. E. *Atomic Energy Levels*, Natl. Stand. Ref. Data Ser. Vol. 35; National Bureau of Standards, Washington, DC, 1911.

(17) Duncan, M. A. *Annu. Rev. Phys. Chem*. **1997**, *48*, 69.

(18) Lessen, D. E.; Asher, R. L.; Brucat, P. J. *Advances in Metal and Semiconductor Clusters*; Duncan, M. A., Ed.; JAI Press: Greenwich, CT, 1993; Vol. 1, p 267.

(19) Castleman, A. W., Jr.; Wei, S. *Annu. Rev. Phys. Chem*. **1994**, *45*, 685.

(20) Farrar, J. M. *Cluster Ions*; Ng, C. Y., Baer, T., Powis, I., Eds.; Wiley: New York, 1993; p 243.

(21) (a) Qian, J.; Midley, A. J.; Donnelly, S. G.; Lee, J. I.; Farrar, J. M. *Chem. Phys. Lett*. **1995**, *244*, 414. (b) Sperry, D. C.; Midey, A. J.; Lee, J. I.; Qian, J.; Farrar, J. M. *J. Chem. Phys*. **1999**, *111*, 8469.

(22) (a) Ding, L. N.; Young, M.; Kleiber, P. D.; Stwalley, W. C.; Lyyra, A. M. *J. Phys. Chem*. **1993**, *97*, 2181. (b) Cheng, C. Y.; Chen, J.; Ding, L. N.; Kleiber, P. D.; Liu, D. K. *J. Chem. Phys*. **1996**, *104*, 6452. (c) Chen, J.; Cheng, Y. C.; Kleiber, P. D. *J. Chem. Phys*. **1997**, *106*, 3884.

(23) (a) Yeh, C. S.; Willey, K. F.; Robbins, D. L.; Duncan, M. A. *Int. J. Mass Spectrom*. **1994**, *131*, 307. (b) France, M. R.; Pullins, S. H.; Duncan, M. A. *Chem. Phys*. **1998**, *239*, 447.

(24) (a) Misaizu, F.; Sanekata, M.; Tsukamoto, K.; Fuke, K.; Iwata, S. *J. Phys. Chem*. **1992**, *96*, 8259. (b) Misaizu, F.; Sanekata, M.; Fuke, K.; Iwata, S. *J. Chem. Phys*. **1994**, *100*, 1161. (c) Sanekata, M.; Misaizu, F.; Fuke, K. *J. Chem. Phys*. **1996**, *104*, 9768.

(25) Yang, X.; Hu, Y. H.; Yang, S. H. *Chem. Phys. Lett.* **2000**, *322*, 491.

(26) (a) Lu, W. Y.; Yang, S. H. *J. Phys. Chem*. A **1998**, *102*, 825. (b) Hu, Y. H.; Yang, X.; Yang, S. H. *J. Chem. Phys*. **1999**, *111*, 134. (c) Yang, X.; Hu, Y. H.; Yang, S. H.; Loy, M. *J. Chem. Phys*. **1999**, *111*, 7837. (d) Yang, X.; Liu, H. C.; Yang, S. H. *J. Chem. Phys.* **2000**, *113*, 3111.

(27) *CRC Handbook of Chemistry and Physics*, 77th ed.; Lide, D. R., Eds.; CRC Press: London, 1996.

(28) Calculated from the bond dissociation energies (BDE) of $X-CH_3$ (X = F, Cl) and Mg^+-X. The BDEs of Mg^+-X are obtained from our ab initio calculations (see text). The accuracy of the calculations was tested on the BDEs of Mg−X, for which the calculated results and the literature data are in excellent agreement (Expt: $D_0(MgF) = 4.75$ eV, $D_0(MgF) = 3.3$ eV (ref 23); Calcd.: $D_0(MgF) = 4.82$ eV, $D_0(MgF) = 3.26$ eV).

(29) France, M. R.; Pullins, S. H.; Duncan, M. A. *Chem. Phys*. **1998**, *239*, 447.

(30) (a) Willey, K. F.; Cheng, P. Y.; Taylor, T. G.; Bishop, M. B.; Duncan, M. A. *J. Phys. Chem*. **1990**, *94*, 4769. (b) Willey, K. F.; Cheng, P. Y.; Bishop, M. B.; Robbins, D. L.; Duncan, M. A. *J. Am. Chem. Soc*. **1991**, *113*, 4721. (c) Willey, K. F.; Yeh, C. S.; Rubbins, D. L.; Duncan, M. A. *J. Phys. Chem*. **1992**, *96*, 9106.

(31) Chen, J.; Wong, T. H.; Kleiber, P. D.; Yang, K. H. *J. Chem. Phys*. **1999**, *110*, 11798.

(32) . (a) Bauschlicher, C. W.; Partridge, H.; Langhoff, S. R. In *Advances in Metal and Semiconductor Clusters*; Duncan, M. A., Ed.; 1994; JAI Press: Greenwich, CT; Vol. 2, p 165. (b) Bauschlicher, C. W. *Chem. Phys. Lett*. **1993**, *201*, 11. (c) Sodupe, M.; Bauschlicher, C. W. *Chem. Phys. Lett*. **1993**, *203*, 215. (d) Bauschlicher, C. W.; Sodupe, M. *Chem. Phys. Lett*. **1993**, *214*, 489. (e) Sodupe, M.; Bauschlicher, C. W.; Patridge, H. *Chem. Phys. Lett*. **1992**, *192*, 185. (f) Sodupe, M.; Bauschlicher, C. W. *Chem. Phys. Lett*. **1992**, *195*, 494. (g) Bauschlicher, C. W.; Sodupe, M.; Partridge, H. *J. Chem. Phys*. **1992**, *96*, 4453. (h) Bauschlicher, C. W.; Partridge, H. *J. Phys. Chem*. **1991**, *95*, 969. (i) C. W. Bauschlicher, C. W.; Partridge, H. *J. Phys. Chem*. **1991**, *95*, 3946.

(33) (a) Breckenridge, W. H.; Jouvet, C.; Soep, B. *Advances in Metal and Semiconductor Clusters*; Duncan, M. A., Ed.; JAI Press: Greenwich, CT, 1995; Vol. 3, p 1; (b) Bondi, A. *J. Phys. Chem*. **1964**, *68*, 441.

(34) Guerra, M. *Chem. Phys. Lett*. **1990**, *167*, 315.